Journal of New Technology and Materials (JNTM)
J. New Technol. Mater.
Vol. 13, N°01 (2023)57-69

OEB Univ. Publish. Co.

Predicting and analyzing of tribo-performance of NAO friction composites using Taguchi Method

F. Yusubov

Department of Materials Science and Processing Technologies, Azerbaijan State Oil and Industry University, Baku, Azerbaijan.

email: fikratyusub@gmail.com
Received date: Feb. 08, 2023; accepted date: May 09, 2023

Abstract

The present study is aimed to investigate the dry sliding behavior of phenolic friction brake pad materials for industrial applications. Low metallic phenolic friction composites with the addition of copper-graphite (Cu-C) particles produced by traditional powder metallurgy methods. The friction test is carried out by pin-on-disc configuration on a universal tribometer MMW-1 with hardened steel as a counterface material. The plan of experiments conducted by Taguchi's L27 orthogonal array on MINITAB 19.1.1 software using a 3-level design model. Analysis of variance (ANOVA) was performed for predicting and analyzing the effect of design parameters like contact pressure (1.9, 5.75 and 9,6 MPa), sliding velocity (0.64, 1.57 and 2.5 m/s) and filler content (5, 10 and 15%) to tribological properties. Results of modeling and optimization of composites have shown that contact pressure has the greatest impact on the friction process following sliding distance and filler content. On the other hand, the most influential factor for the wear process was the sliding velocity, following contact pressure and finally filler content. It was determined that 5-10 Wt.% Cu-C filler content has an effective impact on tribological properties. The friction surface examination of the pin specimens using a scanning electron microscope (SEM) revealed that Cu-C content has a significant effect on improving the heat resistance properties of composites.

Keywords: Brake pad; Non-asbestos; Copper; Graphite; Taguchi; Frictional Heat

1. Introduction

One of the most important parts of brake mechanisms is the brake pad or lining materials. The brake pad function is to either slow down or completely stop the movement by creating a frictional resistance against the rotating element of the device during the braking process [1]. The reliable operation and productivity of automobiles and industrial applications are determined by the work of the brake systems [2]. The main requirement for friction materials in tribotechnical systems is to ensure the rapid conversion of energy into heat and to meet complex requirements such as friction and keeping the stability of tribological properties during multiple braking operations [3]. Higher friction and lower wear characteristics, noise and vibration minimization are considered to be the main norms when designing materials for braking systems [4, 5]. The high wear resistance during friction contact and keeping its initial physical and mechanical properties, as much as possible, at rising temperatures allow these materials to work in operating conditions of heavy load [6]. Although wear is inevitable at the contact of two solids, it is possible to minimize wear through various properties-enhancing elements. Therefore, to meet the growing industrial demands there was always a need to study new materials. Composite materials have become a common material for various industries fields due to their unique properties [7]. The brake friction materials are the most complicated structured among composite materials, consisting of multiphase constituent elements such as binders, fillers, modifiers and fibers [8]. Friction composites are mainly consisting of metallic and non-metallic components. Choosing the right composition is an important factor in the design of modern friction materials for improving tribological properties. Achieving the required friction performance depends on the selection of suitable ingredients. The manufacturing and synthesis of these materials cannot be performed by methods generally accepted for other traditional materials, as in the case of melting, the mixing and integration of the ingredients must be provided with defined parameters [9]. Although polymers have not proved themselves in the industry enough as friction material, recent studies by researchers have shown the possibility to obtain completely new properties using nano-scale particles and various functional fillers [10,11]. One of the most promising materials in terms of economically and environmentally that can meet the requirements of the braking system is polymer-based friction composite materials [12]. Due to these properties, polymer-based powder composite materials containing metal elements can be considered an ideal candidate to work in extreme operating conditions. Metal elements not only increase the required mechanical properties but also have the ability to improve the friction properties [13]. The role of copper and graphite as solid lubricants in

brake friction materials is already studied by different researchers. An increase in graphite content reduces the coefficient of friction but depending on the shape and size, it also increases the wear resistance [14]. Copper increases thermal conductivity, improves sliding properties for different braking regimes [10]. As the nanocrystals on the surface recrystallize at high temperatures, a new brittle friction layer is forming, which acts as a solid lubricant, like graphite. Although the new friction layer reduces the coefficient of friction, it eventually mixes with other worn particles released from the contact area of the disc and brake pad, stabilizing the tribological properties [15]. However, the copper-graphite (Cu-C) effect is not studied as well and it has a particular interest in terms of studying surface characteristics. The characteristics of the contact surfaces are very important for friction materials. The surface roughness of the contacting materials is not only related to the nature of the mechanical properties of the material, but also to the friction and wear process itself. Along with depending on the type of rubbing pair materials, as result of interaction effects such as adhesion, surface fatigue, abrasive wear and tribochemical reactions in the contact surface also influence friction and wear mechanisms of tribological materials [16]. It is known that the process of friction of metallic materials is often characterized by plastic deformation and oxidation wear [17]. Besides, at elevated temperatures friction layer formation, degradation and decomposition of non-asbestos organic (NAO) also influence tribological properties [18, 19]. However, the simultaneous occurrence of several wear mechanisms makes it difficult to assess the friction process and requires a systematic approach.

In order to study these conflicting properties, the design of experiments (DOE) can be helpful. Taguchi approach is a widely used powerful statistical technique for multifactoral experiments (Taguchi and Konishi, 1987). Unlike traditional DOE methods, Taguchi technique uses "smaller-is-better", "larger-the-better" or "nominal-the-better" criteria for achieving the best quality performance and allows evaluate the robustness of the process with numerous approaches [20]. The technique may be more valuable when selected control parameters are discrete and substantiated [21].

In the present study, produced friction composites with Cu-C particles subjected to the analyzing effect of the control parameter and the interactions on friction coefficient and wear rate behaviours. The selected design parameters and their levels were determined based on the commercial materials used in the industry.

2. Materials and methods

2.1. Fabrication of composites

The friction brake pad composites were fabricated using traditional powder metallurgy methods. Three specimens containing eleven ingredients were produced by ball milling, mechanical mixing in dry conditions (for 16 hours with a speed of 60 cycles/min on a horizontal drum mixer), pre-forming at 10 MPa and hot pressing for 20 min. at 160°C under 25.5 MPa pressure.

The glycerin is used as a plasticizer for improving powder processing. The manufacturing process is finished with the post-curing procedure in a muffle furnace for 5 hours in 140°C. The information about formulations of produced specimens formulation is given in Table 1.

Table 1: The Composition of brake pad samples (wt.%)

Sample codes	CG-5	CG-10	CG-15
Copper-graphite	5	10	15
Barite (balance)	28	23	18
Base composition	67	67	67

Base composition consists of following weight proportions: wollastonite (synthetic), 5%, aluminum dioxide 7%, lead 10%, tin 10%, silicon dioxide 7%, modified phenolic resin 25% and additionally, 1% molybdenum disulfide, magnesium oxide and brass particles. The copper-graphite particles obtained by the electrochemical method with grade GK-3 graphite (GOST 17022–76) with a grain size of 100–160 μm. The electrolyte consisted of: 89.2% $CuSO_4 \cdot 5H_2O$, 0.06% Fe, 0.015% As, and 25% sulfuric acid H_2SO_4 (15–45 g/L of concentrated solution) [22]. The base composition (67% Wt.%) was kept constant and Cu-C content was used in three proportions (5, 10 and 15 Wt.%). The remaining composition was compensated with barite filler. Specimens were fabricated in cylindrical pin form in size of Ø 4.7 x 12.8 mm (Fig. 1a). Brake pad composites codes called CG-5, 10 and 15 represent specimens containing 5, 10 and 15 Wt.% Cu-C particles respectively.

a) b)

Figure 1. a) Cylindrical specimens and b) disc used in friction tests

2.2 Plan of experiments

In this study, MINITAB 19.1.1 software used to analyze and correlate responses between different variances. L27 (33) orthogonal array was chosen to design the planning matrix according to the Taguchi technique. Analysis of variance (ANOVA) was performed with 95% confidence level. Three control factors were used to study the friction and wear performance of the composite materials: contact pressure (A), sliding velocity (B), and filler content (C). Each control level combination was repeated three times and the data evaluation was based on obtained average test results.

Information on factors and selected levels are presented in Table 2.

Table 2: Design factors and their levels

Design factors	Code	Unit	Level I	Level II	Level III
Contact pressure	A	MPa	1.9	5.75	9.6
Sliding velocity	B	m/s	0.64	1.57	2.5
Filler content	C	Wt.%	5	10	15

The levels of contact pressure and sliding velocity are determined by testing of analog material Retinax B (FK-24A) (GOST 10851-94) under laboratory conditions. Retinax B (FK-24A) is a commonly used asbestos brake pad material for industrial application, especially for medium and heavily loaded tribotechnical systems.

DOE was conducted mainly in five stages for estimating quality characteristics:

- Signal-to-noise (S/N) calculation
- ANOVA statistical analysis
- Obtaining linear regression model & checking adequacy of the model
- Optimization process parameters
- Confirmation test

The friction coefficient S/N ratio was calculated by setting a goal of the experiment to "larger-the-better" and the wear rate S/N ratio was calculated using "smaller-is-better" criteria. S/N ratios friction and wear were determined using logarithmic loss function (1) and (2) respectively.

$$\frac{S}{N} = -10\log\left[\frac{1}{n}\sum_{i=1}^{n}\frac{1}{y_i^2}\right] \quad (1)$$

$$\frac{S}{N} = -10\log\left[\frac{1}{n}\sum_{i=1}^{n}y_i^2\right] \quad (2)$$

where y is the response for the given factor level, n is the number of experiments.

2.3 Friction and wear test

The dry sliding friction tests were performed on a vertical MMW-1 tribometer with a "pin-on-disc" configuration at room temperature (25°C). The principle of friction tests is based on the simultaneous clockwise rotating of three cylindrical pin samples on a stationary steel disc (Fig. 2). The load applied to the disc by the movement of the rotor which is installed at the bottom part of the machine.

The quenched steel (hardness: 44-46HRC, surface roughness: ~ 0.2 μm) with an outer diameter of 31.7 mm, an inner diameter of 16 mm and a thickness of 10 mm was used as the counter-face material.

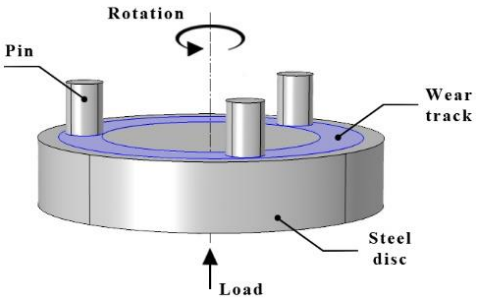

Figure 2. Schematic of pin-on-disc configuration

Prior to each test, the surface of the disc and specimens was cleaned with ethyl alcohol to prevent lubrication. The surface of the specimens was grounded on a polishing machine with 100, 1000 and 2000-grid SiC papers. Worn samples were weighed on an electronic balance (Mettler Toledo) with an accuracy of ± 0.1 mg. The sliding distance was 1.5996 km for all tests.

The following formula was used to calculate the wear rates using weight loss measurements:

$$J = \frac{m_1 - m_2}{\tau} \quad (3)$$

where m_1 and m_2 are the mass before and after wear respectively (gram), τ is the duration of the experiment (hours), and J is the wear rate (g/hour).

3. Results and Discussion

3.1 Signal-to-noise (S/N) calculation

Taguchi generated design with three factors namely contact pressure (A), sliding velocity (B), and filler content (C) at three levels is used for conducting experiments. Table 3 exhibits the experimental results of tribotechnical tests based on the selected planning matrix and calculated S/N ratio values in accordance with the obtained data. Based on the S/N result, it is possible to determine which is the most influential factor in increasing the coefficient of friction. The average S/N values for each factor level are given in Tables 4 and 5. As can be seen from the results, the contact pressure is the most significant factor influencing the change in the coefficient of friction followed by sliding velocity and filler content, respectively. In contrast to the coefficient of friction, the most significant factor influencing the wear rate was the sliding velocity followed by contact pressure and filler content, respectively (Table 5).

Table 3: Experimental test output for L_{27} orthogonal array design

№	Contact pressure (MPa)	Sliding velocity (m/s)	Filler content (Wt. %)	Friction		Wear	
				Friction coefficient (μ)	S/N ratio (dB)	Wear rate (g/hour)	S/N ratio (dB)
1.	1.9	0.64	5	0.403 ± 0.002	-7.89390	0.003 ± 0.001	50.4576
2.	1.9	0.64	10	0.409 ± 0.001	-7.76553	0.008 ± 0.002	41.9382
3.	1.9	0.64	15	0.395 ± 0.003	-8.06806	0.014 ± 0.002	37.0774
4.	1.9	1.57	5	0.391 ± 0.001	-8.15646	0.019 ± 0.001	34.4249
5.	1.9	1.57	10	0.396 ± 0.004	-8.04610	0.026 ± 0.001	31.7005
6.	1.9	1.57	15	0.385 ± 0.002	-8.29079	0.032 ± 0.002	29.8970
7.	1.9	2.5	5	0.375 ± 0.003	-8.51937	0.039 ± 0.003	28.1787
8.	1.9	2.5	10	0.380 ± 0.003	-8.40433	0.046 ± 0.002	26.7448
9.	1.9	2.5	15	0.367 ± 0.002	-8.70668	0.053 ± 0.001	25.5145
10.	5.75	0.64	5	0.425 ± 0.003	-7.43222	0.012 ± 0.002	38.4164
11.	5.75	0.64	10	0.431 ± 0.001	-7.31045	0.019 ± 0.001	34.4249
12.	5.75	0.64	15	0.417 ± 0.002	-7.59728	0.027 ± 0.001	31.3727
13.	5.75	1.57	5	0.412 ± 0.002	-7.70206	0.024 ± 0.003	32.3958
14.	5.75	1.57	10	0.417 ± 0.003	-7.59728	0.032 ± 0.002	29.8970
15.	5.75	1.57	15	0.393 ± 0.001	-8.11215	0.041 ± 0.002	27.7443
16.	5.75	2.5	5	0.396 ± 0.002	-8.04610	0.034 ± 0.001	29.3704
17.	5.75	2.5	10	0.403 ± 0.005	-7.89390	0.043 ± 0.003	27.3306
18.	5.75	2.5	15	0.388 ± 0.006	-8.22337	0.052 ± 0.001	25.6799
19.	9.6	0.64	5	0.441 ± 0.003	-7.11123	0.029 ± 0.001	30.7520
20.	9.6	0.64	10	0.445 ± 0.004	-7.03280	0.035 ± 0.004	29.1186
21.	9.6	0.64	15	0.439 ± 0.003	-7.15071	0.042 ± 0.002	27.5350
22.	9.6	1.57	5	0.436 ± 0.003	-7.21027	0.035 ± 0.003	29.1186
23.	9.6	1.57	10	0.440 ± 0.002	-7.13095	0.044 ± 0.002	27.1309
24.	9.6	1.57	15	0.431 ± 0.002	-7.31045	0.054 ± 0.001	25.3521
25.	9.6	2.5	5	0.412 ± 0.002	-7.70206	0.046 ± 0.004	26.7448
26.	9.6	2.5	10	0.416 ± 0.005	-7.61813	0.058 ± 0.005	24.7314
27.	9.6	2.5	15	0.395 ± 0.003	-8.06806	0.069 ± 0.001	23.2230

Table 4: Response table for S/N ratios for friction coefficient

Level	Contact pressure (MPa)	Sliding velocity (m/s)	Filler content (Wt. %)
1	33.99	35.68	33.32
2	30.74	29.74	30.34
3	27.08	26.39	28.16
Delta (Δ)	6.91	9.29	5.16
Rank	2	1	3

Table 5: Response table for S/N ratios for wear rate

Level	Contact pressure (MPa)	Sliding velocity (m/s)	Filler content (Wt. %)
1	-8.206	-7.485	-7.753
2	-7.768	-7.729	-7.644
3	-7.371	-8.131	-7.948
Delta (Δ)	0.835	0.647	0.303
Rank	1	2	3

Fig. 3a and b show the control factor dependence graphs of S/N ratios values for the friction coefficient and wear rate, respectively. Delta (Δ) is the average difference between the maximum and minimum response values for each factor.

Taguchi suggests that response with a large S/N ratio indicates its importance on the process. As can be seen from Fig. 3, graphs whose starting and ending points are farther from the horizontal line show that they have a greater effect. The graphs demonstrate that the most important factor influencing the increase in the coefficient of friction is the contact pressure. The most important factor influencing the wear rate is the sliding velocity.

The obtained curves reflect the given values in Tables 4 and 5 and demonstrate the most significant factor effects. Defined impact ranges for both response values helped to determine the optimal regime parameters.

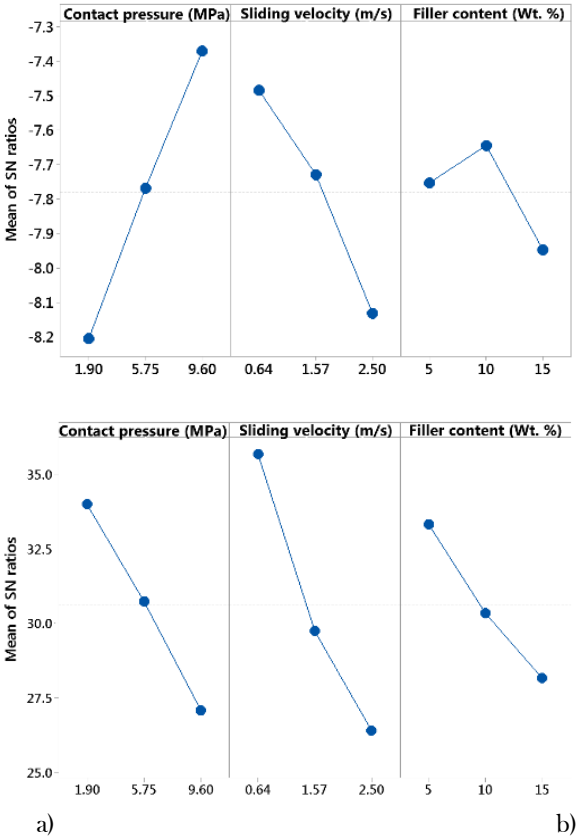

a) b)

Figure 3. Main effects plot for S/N ratios of a) friction coefficient and b) wear rate

3.2 Statistical analysis (ANOVA)

Processing of experimental test results by ANOVA helped to identify the factors affecting the coefficient of friction (Table 6). As can be seen from Table 6, the P-values of the friction coefficient are zero for the main factors, which shows their statistical significance, but the α-value of each of the interaction factor conditions was higher than 0.05.

Table 6: Analysis of variance (ANOVA) table for friction coefficient

Source	DF	Seq SS	Adj SS	Adj MS	F-value	P-value	P, %
Contact pressure (A)	1	0.006962	0.001660	0.001660	91.24		55.75%
Sliding velocity (B)	1	0.004140	0.000001	0.000001	0.06	0.809	33.16%
Filler content (C)	1	0.000364	0.000439	0.000439	24.14		2.92%
B*B	1	0.000078	0.000078	0.000078	4.30	0.052	0.63%
C*C	1	0.000554	0.000554	0.000554	30.46		4.44%
A*B	1	0.000024	0.000024	0.000024	1.32	0.264	0.19%
B*C	1	0.000019	0.000019	0.000019	1.03	0.323	0.15%
Error	19	0.000346	0.000346	0.000346			2.77%
Total	26	0.012488	0.001660	0.001660			100.00%

Table 7: Analysis of variance (ANOVA) table for wear rate

Source	DF	Seq SS	Adj SS	Adj MS	F-value	P-value	P, %
Contact pressure (A)	1	0.001644	0.000278	0.000278	27.99		24.53%
Sliding velocity (B)	1	0.003500	0.000503	0.000503	50.66		52.24%
Filler content (C)	1	0.001136	0.000027	0.000027	2.69	0.117	16.96%
A*B	1	0.000176	0.000176	0.000176	17.76		2.63%
A*C	1	0.000024	0.000024	0.000024	2.43	0.135	0.36%
B*C	1	0.000021	0.000021	0.000021	2.15	0.158	0.32%
Error	20	0.000199	0.000199	0.000010			2.96%
Total	26	0.006700					100.00%

DF-degrees of freedom, Seq SS-sequential sum of squares, Adj SS-adjusted sum of squares, P-percentage of contribution

Significance levels below α = 0.05 indicate their significance is low. Thus, the higher the value of F, the higher the effect on the process, and according to this principle, the impact percentage is determined in the following order. Contact pressure is the most significant parameter with the highest percentage contribution (55.75%), following sliding velocity (28.48%), and finally filler content (2.92%). The most important of the interaction factors was the combination of filler content - filler content (C*C), which was 4.44%. The percentage of factors influencing the wear rate is determined in the following order (Table 7). The most dominant factor is sliding velocity (52.24%), following contact pressure (24.53%) and filler content (16.96%). The most important of the interaction factor conditions was the combination of contact pressure - sliding velocity (A*B) at 2.63%. The Pareto chart can be useful to better understand the effect of interactions. Fig. 4. shows the Pareto chart for the main factors and their combinations. In both graphs reference line is 2.11. This shows that the factors crossing the reference line are statistically significant at the 0.05 level for the given model. The graphs show that the contact pressure and sliding velocity are the most influential factors for both output parameters. However, the Pareto chart does not show which factors increase or decrease the response.

Based on the results obtained, a 3D interpretation of the dependence of the friction coefficient and wear rate on the regime parameters is given in Figs. 5 and 6, respectively. As can be seen from Pareto charts, factor C (filler content) is the least important among the main factors. Therefore, in order to understand better the effect of process parameters on changes of response values, material factor (C) is not taken into account in 3D plots. As can be seen from Fig. 5, the increase in sliding velocity reduces the frictional characteristics of the material. This is due to the increased intensity of wear rate at high sliding velocity (Fig. 6).

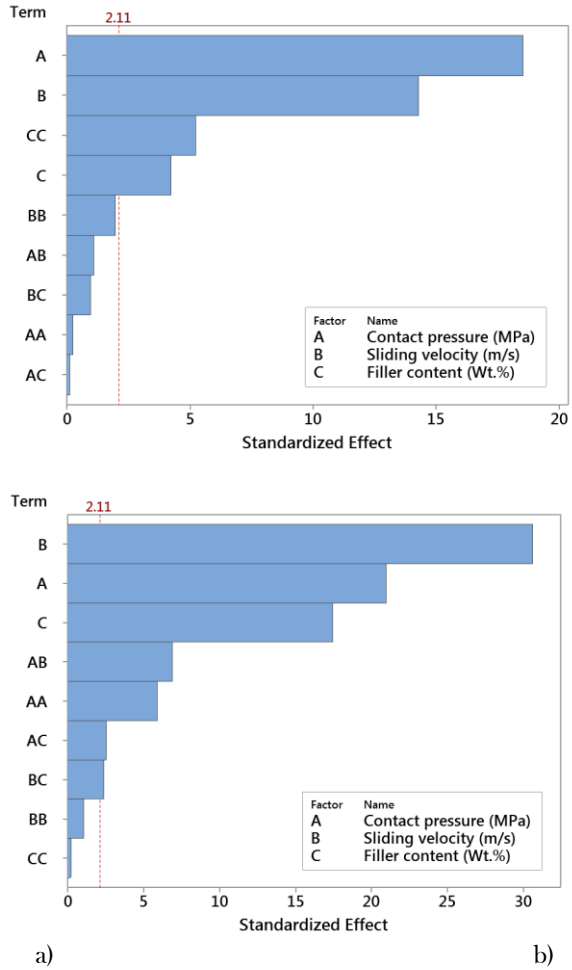

a) b)

Figure 4. Pareto chart of the standardized effects for a) friction coefficient and b) wear rate

Changes in the contact surface as a result of wear lead to a decrease in the coefficient of friction. This dependence can be better seen in Figs 9 and 10.

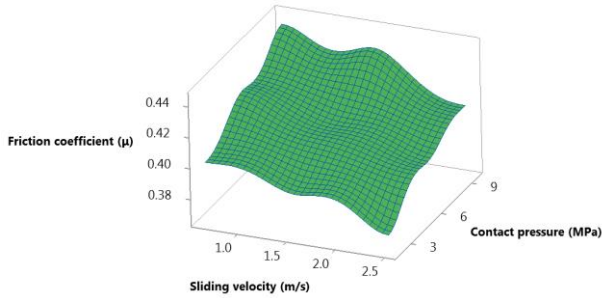

Figure 5. Surface plot for dependence between friction coefficient and regime parameters

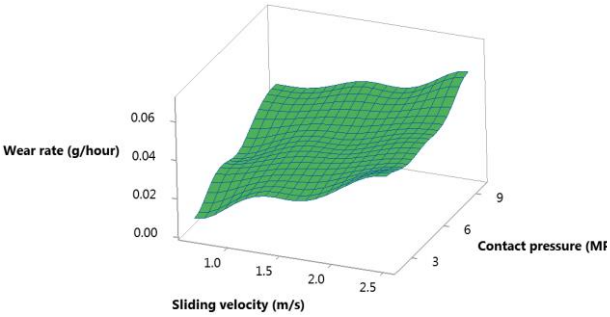

Figure 6. Surface plot for dependence between wear rate and regime parameters

During sliding, material removal or gain occurs due to interactions between two solid surfaces. In the initial phase of sliding distance meeting of contact surfaces with each other, mainly resulting in plastic deformation. The occurrence of plastic deformation leading to the transformation of mechanical energy into frictional heat. Under frictional force in the surface of heterogeneous structured brake pads materials, primary and secondary contact plateaus are forming [23]. In a closer look, if we approach it on a nano-scale, it is known those friction surface asperities are very rough. During the first stage of friction under big contact stress, harder asperities of the disc break off softer brake pad asperities and form new real contact areas. Although the increase in the real contact areas has a positive effect on the friction characteristics, the structure of the contact surfaces changes again as a result of wear [24, 31]. For this reason, the highest coefficient of friction was at a contact pressure of 9.6 MPa and a sliding speed of 0.64 m/s (0.445). The coefficient of friction began to decrease more intensively after ~1.5 m/s. Kragelski, I. V. (1962) attributed the decrease in the coefficient of friction with the increase in the sliding velocity to the weakening of the formation of a strong bond between the two friction surfaces due to generated oxide layer. This is a phenomenon related to the mechanical properties of materials and may have different effects on friction depending on the properties of the individual components. Simultaneously, increasing the sliding velocity also increases the frictional temperature at pairing surfaces. Generated heat during the friction process increases interface temperature, which is resulting in a decrease in the friction coefficient [25]. As the temperature rises, changes in the tribological behavior of contact materials occur. A great amount of dissipated energy flow is absorbed by the brake pad and affecting material properties. The high temperature generated on the contact surface is distributed from the interface layer into the material. The distribution of temperature within a material depends on the thermo-physical characteristics of that material [26]. At the end of the friction tests, two models of thermal effects were identified in the samples, especially in high contact and sliding velocity conditions. A graphical description of observed heat effects based on the cross-section of the specimens is given in Fig. 7a [27].

The first model (Fig. 7a) describes the completely burned contact surface of the sample with low filler content (CG-5). This can be understood as the low thermal conductivity of the CG-5 sample, due to the low content of copper-graphite. In samples CG-10 and 15, no significant difference was found in the contact surface and the other parts. This effect shows that heat is rapidly distributed and transferred within these materials, which also indicates a possible increase of thermal conductivity by Cu-C particles [27].

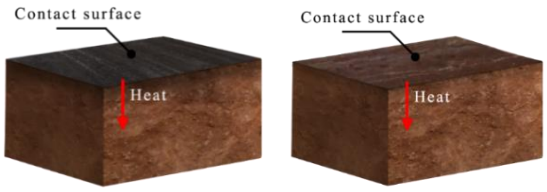

a) b)

Figure 7. Frictional heat effect on specimen a) CG-5 b) CG-10 and 15

The difference between CG-10 and 15 was only noticeable in images taken with a scanning electron microscope (SEM) (Fig. 8). Fig. 8 shows the SEM observations of worn surfaces of CG-5, 10 and 15. These observations cover 9.6 MPa pressure and 2.5 m/s sliding velocity regimes (except Fig. 8c, it shows worn surface in 9.6 MPa pressure and 0.64 m/s sliding velocity combination). Unlike the CG-15 sample, the number of cracks on the surface of the CG-5 was larger and deeper (Fig. 8b). Due to the low mechanical properties of CG-15, the wear was high and its complex wear mechanism reflected in the surface morphology. However, in the CG-15 sample, an increase in the sliding velocity was observed with microcracks (Fig. 8d). It is also possible to see the deepening of micro-voids, which indicates the intensification of the participation of metal particles such as aluminum oxide and silicon dioxide in the abrasive wear process with the degradation of

organic components. Signs of plastic deformation are also visible in various areas of the friction surface which indicates that high Cu-C content affected the surface structure (Fig. 8c and d). Oxidation of Cu as a result of local temperature increase can influence wear mechanism by forming tribo-layer [28]. Oxidation influences were not observed in CG-15 as much as in CG-5 and CG-10 specimens due to low copper content. Generated heat during friction affects the oxidation, thermal strength and plasticity of the material. This leads to changes in the surface following complicated physical-chemical reactions (diffusion and adsorption of atoms or molecules on the friction surface) [29]. The change in the interaction between the surfaces as a result of structural changes is reflected in the dry frictional behaviour of brake pad composites. Graphs show that the coefficient of friction does not decrease in high contact pressure regimes, on the contrary, an increase is observed (Fig. 5 and 9). This difference is especially noticeable in settings with low sliding velocity and high contact pressure settings.

The reduction of the friction coefficient can be explained by a decrease in the contact time at the asperities due to an increase in speed [30]. Due to the reduction of the contact time, the possibility of forming enough junctions for friction by adhesion is reducing. However, this process may be different depending on the properties of the brake sample surface and friction layer characteristics. When the pressure is high, the heating of the contact surface can cause the formation of a friction layer of solid lubricants, which leads to the stabilization of the coefficient of friction [31].

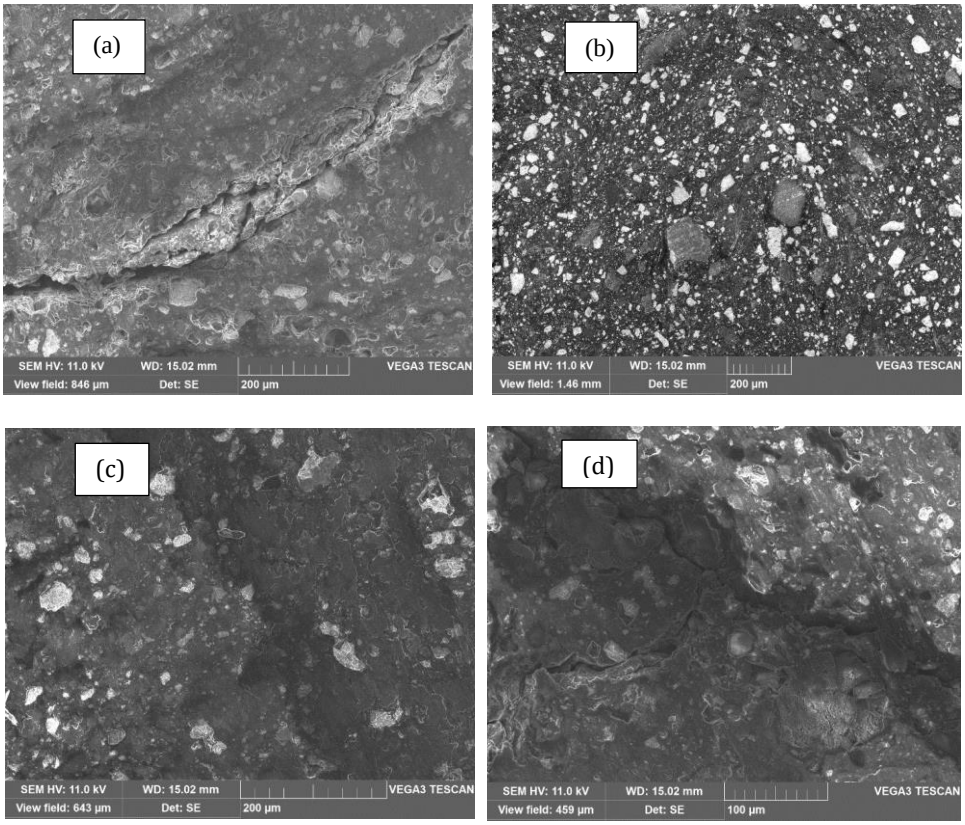

Figure 8. SEM images of worn surfaces of composites a) CG-5, b) CG-10 c) CG-15 (B=0.64 m/s) and d) CG-15

Depending on termo-mechanical properties of material sliding velocity is the leading generation of non-uniform pressures with high local contact stresses in relative motion [32]. These effects are impacting surface morphology and cause non-stability of friction coefficient. The mentioned effects on the friction surface can be seen clearly in Figs 8a and c. Since the wear of the friction layer is not high at low sliding velocity, this prevents the friction coefficient from decreasing over a period of time.

The lowest friction coefficient was observed at a contact pressure of 1.9 MPa and a sliding velocity of 2.50 m/s (0.367) (Fig. 9). Wt.% 15 of filler content in this combination is one of the reasons that reduce friction. This can be attributed to the formation of a copper-graphite lubricating film at the sliding surface. The graphite layer significantly reduces the contact of the specimen with the rotating disc surface. The formed film

thickens due to the worn particles of the sample, further reducing the coefficient of friction.

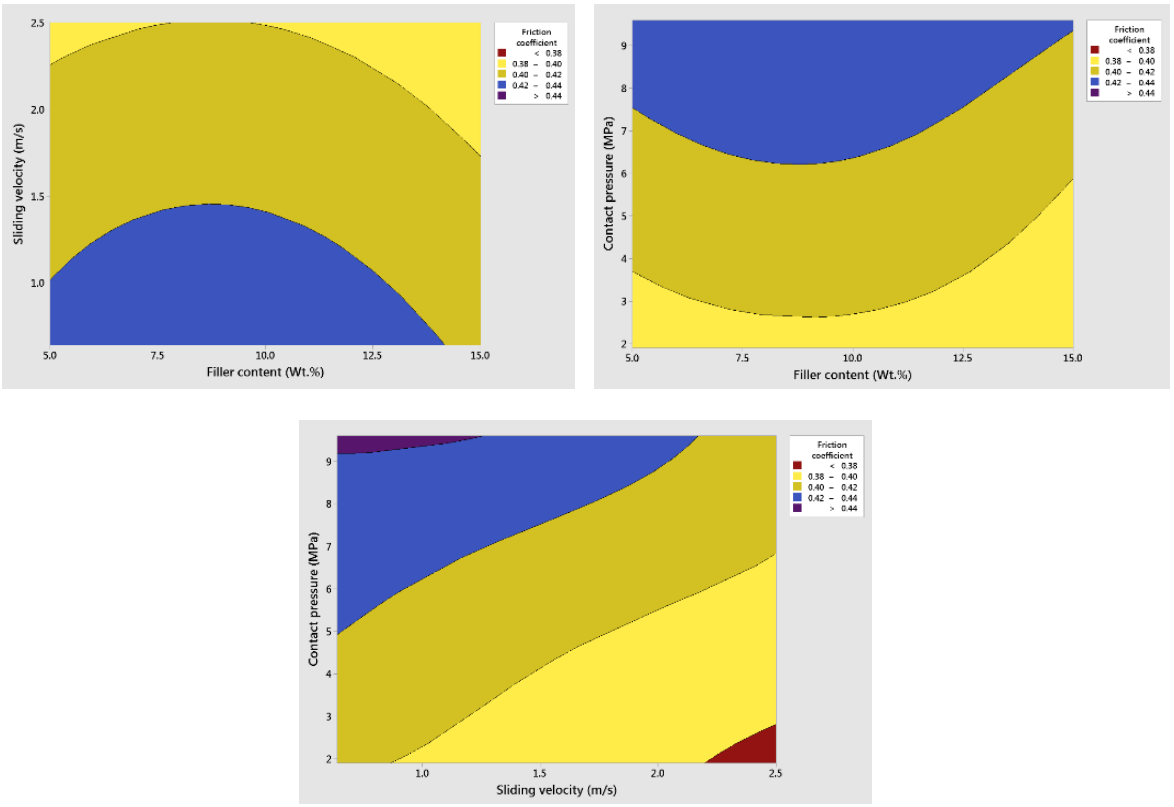

Figure 9. Contour plot for dependence between friction coefficient and regime parameters

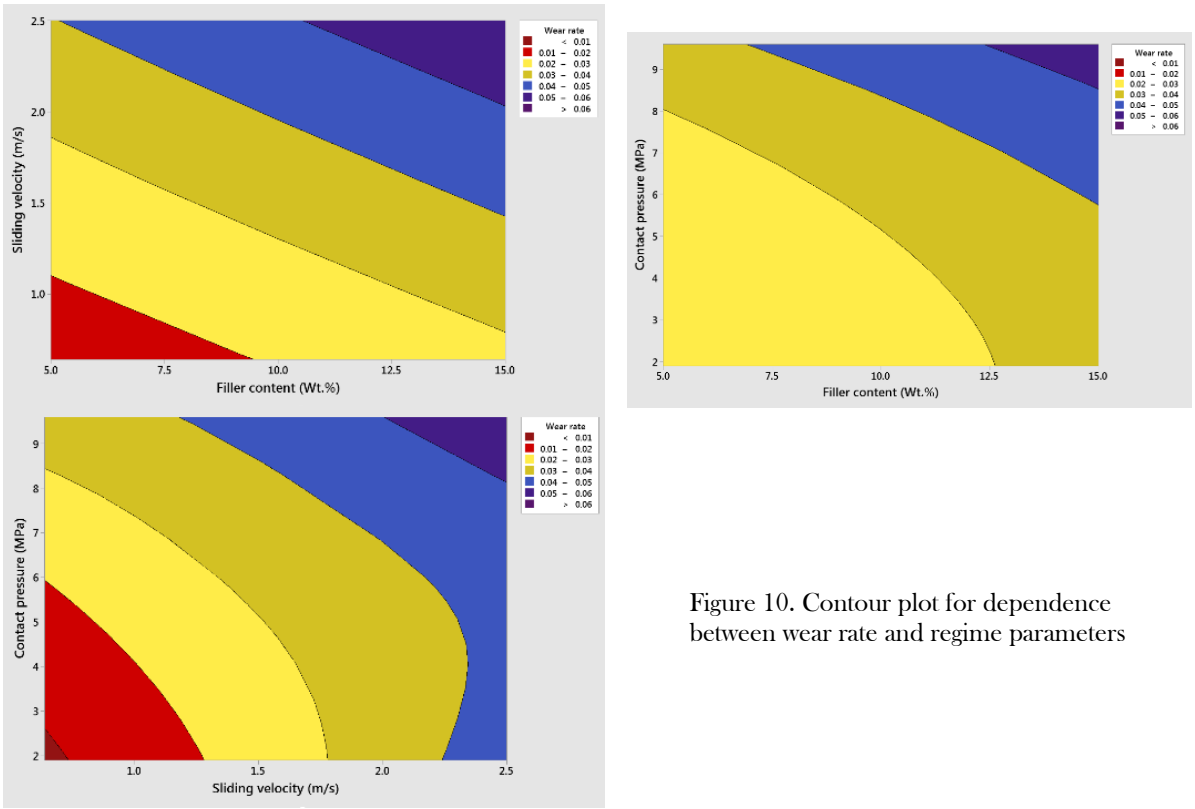

Figure 10. Contour plot for dependence between wear rate and regime parameters

An increase in wear rates was observed in a typical sequence the increase in the contact pressure and sliding velocity resulted in an increase in wear rate. The highest wear rate responses were observed at 9.6 MPa contact pressure and 2.50 m/s sliding velocity conditions (0.068 g/hour). The lowest was observed at a contact pressure of 1.9 MPa and a sliding speed of 0.64 m/s (0.003 g/hour) (Figs. 6 and 10). It should also be noted that contour plots imply that filler content up to 10Wt.% is improving the wear resistance of samples. But 15 Wt.% filler is not appropriate in terms of tribological properties. In CG-15 specimens wear rate values were high in comparison. When the contact pressure is high the graphite particles are squeezed out from the contact area and this leads to an increase in the wear rate [33]. This phenomenon causes a change in the structure of the friction surface. Surface roughness parameters are one main factor which is determining the contact behavior of rubbing pair materials. As discussed above frictional heat formed a surface roughness by changing the surface morphology in the CG-15 brake pad sample (Fig. 8c). During dynamic asperity - asperity contacting, depending on initial surface roughness elastic or a plastic deformation may occur [34]. These tribo-mechanical influences are impacting friction stability and wear of mating brake materials. Thus, surface roughness can also be considered as one of the main reasons for high wear rates in CG-15 specimens.

3.3 Obtaining linear regression equation & cheking adequacy of model

The linear regression equation was applied to establish a correlation between the important factor conditions obtained with based on the ANOVA results, and the following equations (4) and (5) were obtained for the coefficient of friction and wear rate, respectively:

$$\text{Friction coefficient } (\mu) = 0.36633 + 0.005729\,A + 0.00177\,B + 0.00721\,C - 0.00418\,B^{*}B - 0.000384\,C^{*}C - 0.000396\,A^{*}B - 0.000269\,B^{*} \quad (4)$$

$$\text{Wear rate (g/hour)} = -0.01997 + 0.003427\,A + 0.01828\,B + 0.000716\,C - 0.001071\,A^{*}B + 0.000074\,A^{*}C + 0.000287\,B^{*} \quad (5)$$

The positive regression coefficients indicate that response values increase with selected control factors and negative regression coefficients suggest that response values decrease with selected control factors. Information about the coefficients related to the models can be found in Tables 8 and 9.

Table 8: Regression coefficients for friction coefficient

Term	Coef	SE Coef	T-value	P-value
Constant	0.36633	0.00922	39.75	
Contact pressure (A)	0.005729	0.000600	9.55	
Sliding velocity (B)	0.00177	0.00722	0.24	0.809
Filler content (C)	0.00721	0.00147	4.91	
B*B	-0.00418	0.00201	- 2.07	0.052
C*C	-0.000384	-0.000070	- 5.52	
A*B	-0.000396	-0.000344	- 1.15	0.264
B*C	0.000269	-0.000265	- 1.02	0.323

Model summary: S=0.0042659, R^2=97.23%, R^2 (adj)=96.21%

Table 9: Regression coefficients for wear rate

Term	Coef	SE Coef	T-value	P-value
Constant	-0.01997	0.00524	- 3.81	0.001
Contact pressure (A)	0.003427	0.000648	5.29	
Sliding velocity (B)	0.01828	0.00257	7.12	
Filler content (C)	0.000716	0.000436	1.64	0.117
A*B	-0.001071	-0.000254	- 4.21	
A*C	0.000074	0.000047	1.56	0.135
B*C	0.000287	0.000196	1.47	0.158

Model summary: S=0.0031144, R^2=97.04%, R^2 (adj)=96.15%

From equation (3) it is observed that contact pressure plays a major role on the friction coefficient. A number of factor combinations (B*B, C*C, A*B and B*C) were negatively related to the coefficient of friction. This is due to the processes occurring on the friction surface which is discussed above. Equation (4) showed that wear rate highly influenced by sliding velocity and contact pressure. And thus, these factors increase the wear rate of brake pad specimens. Almost all of the selected factors and their combinations contribute to the increase of wear rates. Obtained regression equations can be used to predict tribological behaviours of the brake pad composites. Residuals vs. Fitted Value graphs showing the adequacy of the model obtained by linear regression equations (4) and (5) are given in Fig. 11.

The graph is reflecting the distribution of negative residual values below the zero line, and the positive results above that zero line in the vertical direction along

the ordinate axis. Residual values are calculated by the following formula [35]:

$$e = y - \hat{y} \quad (6)$$

where e is the residual, y is the experimental response value and ŷ is the predicted response value.

According to the accepted distribution patterns, obtained results prove the adequacy of the model. Thus, inadequate models, residual values are usually characterized by random distribution in different directions above and below the zero line (presented in Minitab). For the friction coefficient, the largest deviations in the graph are the results for rows 15, 18 and 27 in the planning matrix given in Table 3 (Fig. 11a). Each of the above-stated rows is containing a sample where the filler content is 15 Wt.%. In specimens from 5 to 10 Wt.% filler content, an error of row 15 occurred due to increased friction and wear.

a)

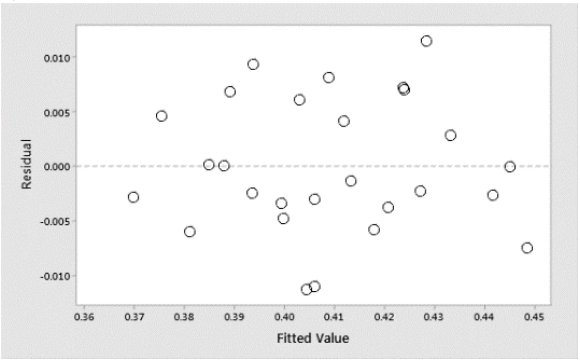

b)

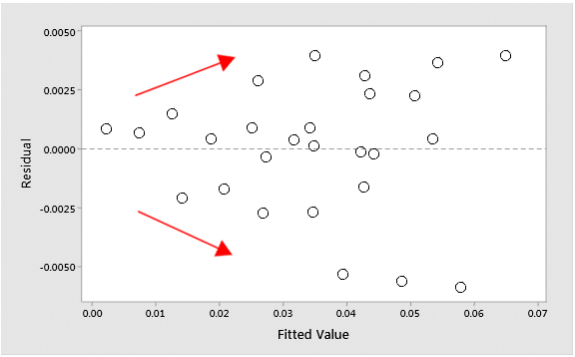

Figure 11. Residual plots of linear regression model for a) friction coefficient and b) wear rate

The plots showing the distribution of the residual between the experimental results and the predicted values for the wear rate also show that this model is adequate for the process (Fig.11b). Despite this, the unequal distribution of residuals can be seen in Fig. 11b. The red arrows show that residuals are increases with fitted response values magnitude. All large residuals are referring to the results for the first starting point of the third level of sliding velocity (2.5 m/s). The residual was higher in these rows because the effects at level 3 of the sliding velocity were different depending on the filler content.

As can be seen from basic information on both models in Tables 8 and 9, 97.23% of the predicted values of the model (3) coincide with the experimental results, which can be considered a satisfactory result. The results of the wear rate were also satisfactory. The coefficient of determination (R^2) for the wear rate (model 4) was 97.04%.

3.4 Optimization process parameters

The results of the optimization for the friction coefficient are given in Fig. 12. In the presented optimization graphs blue lines show optimal settings and black lines show the predicted response values at different regimes. As described in Fig. 9, the optimal friction condition is a combination with a contact pressure of 9.6 MPa, a sliding velocity of 0.64 m/s and a content filler of 10 Wt.%. The predicted value of the friction coefficient in this regime is 0.451898.

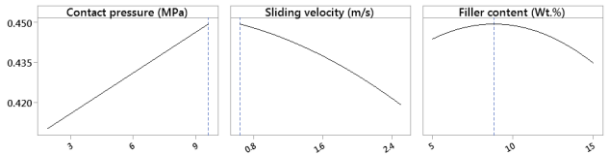

Figure 12. Setting and optimal solution for friction coefficient

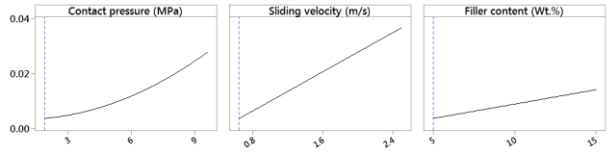

Figure 13. Setting and optimal solution for wear rate

The results of the optimization for the wear rate are given in Fig. 13. As shown in the figure, the optimal condition for the wear is at the lowest level of each factor: the contact pressure is 1.9 MPa, the sliding velocity is 0.64 m/s and the content filler is 10 Wt.%. The predicted value of wear rate in this condition is 0.0020093 g/hour.

3.5 Confirmation test

Checking the accuracy of the results is the last step in the planning methods of experiments. Table 10 exhibits the conditions selected for both response parameters. According to these parameters, the obtained results are given in Tables 11 and 12.

Table 10: Parameters used for confirmation test

Experiments, №	Contact pressure	Sliding velocity	Filler content
1	9.6	2.5	10
2	1.9	0.64	15

Table 11: Confirmation results for friction coefficient

№	Experimental	Predicted	Error (%)
1	0.416	0.418519	0.61
2	0.395	0.395407	0.10

Table 12: Confirmation Results for Wear Rate

№	Experimental	Predicted	Error (%)
1	0.058	0.0558889	3.64
2	0.014	0.0140833	0.60

A comparison of the predicted values with the experimental values according to the regression model showed that the error was less than ~3% for both configurations, which is an acceptable result.

4. Conclusions

Using the Taguchi technique following conclusions are drawn based on statistical processing of obtained data from experimental friction and wear tests:

- P-values of selected design factors were higher than 0.05, which is proves their importance to tribological properties.
- ANOVA results showed that contact pressure (55.75%) and sliding velocity (33.16%) is a most significant factor on the friction coefficient. Filler content impact was only 2.92%.
- Most significant variable on wear rate is the sliding distance (52.24%), then contact pressure (24.53%) and filler content 16.96%.
- The highest friction coefficient (0.445) and lowest wear rate were obtained in brake pad composition containing 10 Wt.% copper-graphite particles.
- The lowest friction coefficient (0.367) and highest wear rate was found in brake pad composition containing 15 Wt.% copper-graphite particles.
- Friction coefficient increasing with the increase of contact pressure with lowest sliding velocity but decreases with the increase of sliding velocity.
- Surface characterization with SEM and graphical scheme for frictional heat effect indicates that copper-graphite particles are increasing of heat conductivity of the composite materials. Brake pad specimen containing 10 Wt.% copper-graphite particles have a better friction surface.
- From generated regression equations it is observed that contact pressure is positively related to process and plays a major role in friction coefficient. Also, the contact pressure and sliding velocity are positively related to the output parameter and serve to increase the wear rate.
- Optimal combination for friction coefficient was determined to be contact pressure 9.6 MPa, sliding velocity 0.64 m/san and optimum conditions for wear rate were typically at the lowest level of parameters.

References

[1] M. Asif, K. Chandra, P. S. Misra, Int. J. Mech. Mater. Eng. 8 (2012) 94-104.

[2] K. W. Liew, U. Nirmal, Mater. Des., 48 (2013) 25–33.

[3] I. Sugözü, I. H. Mutlu, K.B. Sugozu, Polym. Compos. 39 (2015) 55-62.

[4] K. Friedrich Adv Ind Eng Polym Res. 1 (2018) 3-39.

[5] A. Gåård, N. Hallbäck, P. Krakhmalev, Wear, 268 (2010) 968-975.

[6] X. Xiao, Y. Yin, J. Bao, L. Lu and X. Feng, Adv. Mech. Eng. 8 (2016) 1-10.

[7] H. K. Zishan, Recent Trends in Nanomaterials: Synthesis and Properties, Springer, Berlin, 2017.

[8] P.E. Kosbe, P.A. Patil, M. Manickam and G. Ramamurthy, Phys. Sci. 30 (2019) 81–97.

[9] A. Nilov, V. Kulik and A. Garshin, Refrac. Ind. Ceram. 56 (2015) 402-412.

[10] S. Sanjeev, B. Jayashree, and K. Mukesh. Nanomat. Nanotechnol. 3 (2013) 1-9.

[11] K. K. Kamal (Ed.), Composite Materials Processing, Applications, Characterizations; Springer, Berlin, 2017.

[12] P. Ghosh, S. Banerjee and D. Khastgir, Polym. Eng. Sci. 60 (2020) 1-13.

[13] S. Akhtar, M. Saad, M.R, Misbah and M.C. Sati, Materials Processing and characterization, India 16-18 March, 2018; Materials Today: Proceedings, 5 (2018) 18649-18655.

[14] Y. Jiazhi, Z. Jing and D. Zhenxin, IOP Conference Series: Mater. Sci. Eng. 397 (2018) 3 1-7.

[15] M. Kumar and J. Bijwe, Wear, 270 (2011) 269-280.

[16] A.Y. Grigoriev, A.M. Dubravin, A.V. Kovalev, I.N. Kovaleva, O.Y. Komkov and N.K. Myshkin, Wear, 24 (2003) 51-58.

[17] J. Ding, S.B. Leen, E.J. Williams and P.H. Shipway, Proc. ImechE, Part J: J. Eng. Tribol. 223 (2009) 1019-103.

[18] T. Singh, A. Patnaik and B. Gangil, J. Indus. Textiles, 45 (2016) 1335-1349.

[19] G. Lu, X. Shi, Y. Huang, X. Liu and M. Yang Mate. Res. Express, 5 (2018) 1-10.

[20] K.R. Ranjit. Design of Experiments Using the Taguchi Approach: 16 Steps to Product and Process Improvement, John Wiley & Sons, NJ 2001.

[21] M.S. Gujrathi, L.S. Dhamande and P.M. Patare Bonfring I. J. I. E. M. S. 3 (2013) 47-51.

[22] С. М. Мустафаев, А. В. Шарифова, А. А. Гулиев, Прогресивні Технології і Системи

Машинобудування, 1-2 (2013) 187-191. (In Russian)
[23] L.Y. Barros, P.D. Neis, N.F. Ferreira, R.P. Pavlak, D. Masotti, L.T. Matozo, J. Sukumaran, P. De Baets and M. Andó, Wear, 352-353 (2016) 112–121.
[24] S.J. Kim, C.H. Min, K.H. Cho and H. Jang, Tribol. Int. 40 (2007) 15-20.
[25] B. Sugozu, A.N. Daghan, N. Akdemir and N.Ataberk, Indus. Lubrication. Tribol. 68 (2016) 259-266.
[26] J. Bao, Z. Zhu, M. Tong and Y. Yin, Adv. Sci. Let. 4 (2011) 3716-3720.
[27] F. Yusubov, J. Frict. Wear. 41 (2020) 125–128.
[28] M. Z. Akbarpour, S. Alipour, M. Farvizi, and H.S.Kim, Arch. Civ. Mech. Eng. 19 (2019) 19 694-706.
[29] J. Bao, Y. Yin, Z. Zhu, M. Tong, Y. Lu, and Y. Peng, Appl. Compos. Mater. 20 (2012) 331-339.
[30] G. Straffelini, Friction and Wear Methodologies for Design and Control, Springer, Germany, 2015.
[31] P.C. Verma, R. Ciudin, A. Bonfanti, P. Aswath, G. Straffelini and S. Gialanella, Wear, 346-347 (2016) 56-65.
[32] M.O. Petinrin and J.O. Oji, Sci. J. 5 (2012) 39-43.
[33] A. Baradeswarana and A.E. Perumal, Tribo. Trans. 58 (2015) 1–6.
[34] B. Bikramjit and K. Mitjan, Tribology of Ceramics and Composites: a Materials Science Perspective, Wiley, NJ, 2011.
[35] M. Teruo, Taguchi Methods Benefits, Impacts, Mathematics, Statistics, and Application, ASME Press, NJ, 2011.